CHAPTER 4

RECOVERY OF TANTALUM AND SILVER FROM WASTE TANTALUM CAPACITORS

4. RECOVERY OF TANTALUM AND SILVER FROM WASTE TANTALUM CAPACITORS

In this chapter a method was developed for recovery of tantalum and silver from waste tantalum capacitors. The metallic and non-metallic fractions, separated after pre-processing, were processed individually to recover desired metal. Initially results of tantalum recovery are discussed. To recover tantalum from metal-rich concentrate, two different routes were adopted i.e., alkaline leaching and acidic leaching to assess the efficacy of each process route. Alkaline media was used to preferentially dissolve tantalum into the leaching medium followed by purification using solvent extraction, whereas; acidic media was used to dissolve everything in the solution, except tantalum. Since oxide of tantalum exhibits significant acidic properties, due to which it is reluctant to dissolve in dilute acidic solution (Chen et al., 2019; Theron et al., 2011). To take the advantage of this condition, recovery of tantalum was planned using acidic leaching media. After establishing the fact that acidic route is more efficient than alkaline route in terms of recovery efficiency of tantalum, further experiments were continued with acidic media to optimize the leaching parameters i.e., temperature, leachant concentration, pulp density, and time. The results of kinetic studies are also presented where the experimental activation energies for dissolution were calculated as part of studying the reaction mechanism of manganese and nickel dissolution in 1st stage leaching. Finally, towards the end of this chapter the outcomes of silver recovery from non-metallic-rich concentrate is elaborated.

4.1 Characterization of capacitors

Cross-sectional SEM micrograph in *Figure 4.1*a shows the layer wise distribution of metallic and non-metallic fraction in the capacitor. The part of *Figure 4.1*a which shows different layers (bright and dark contrast) was zoomed in *Figure 4.1*b and EDS spectrum

was collected from each layer to identify the manufacturing material. The result of EDS is labeled in *Figure 4.1*b.

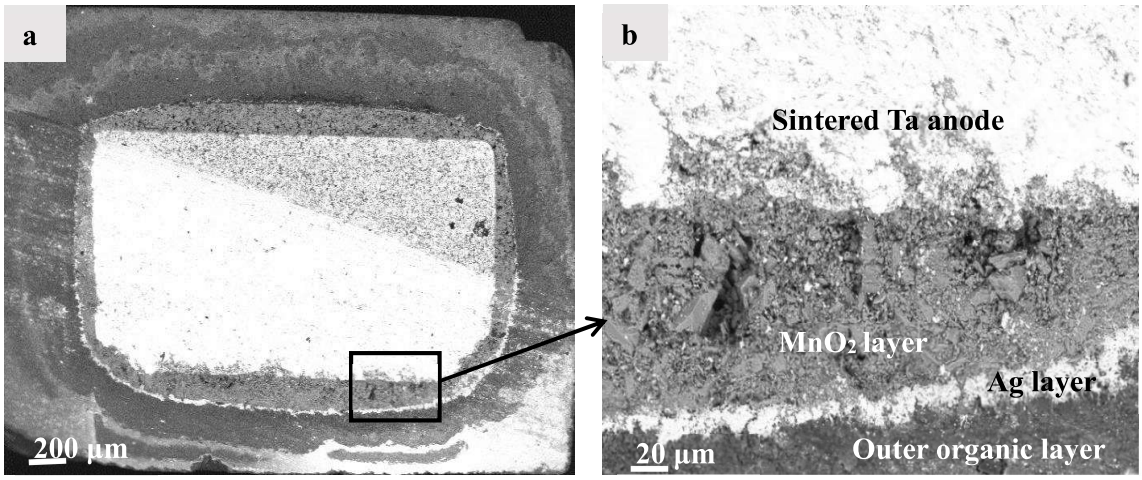

Figure 4.1 Back-scattered electron (BSE) imaging of cross-section of a tantalum capacitor: a) low magnification image showing the full cross section and b) zoomed-in image to show the different layers.

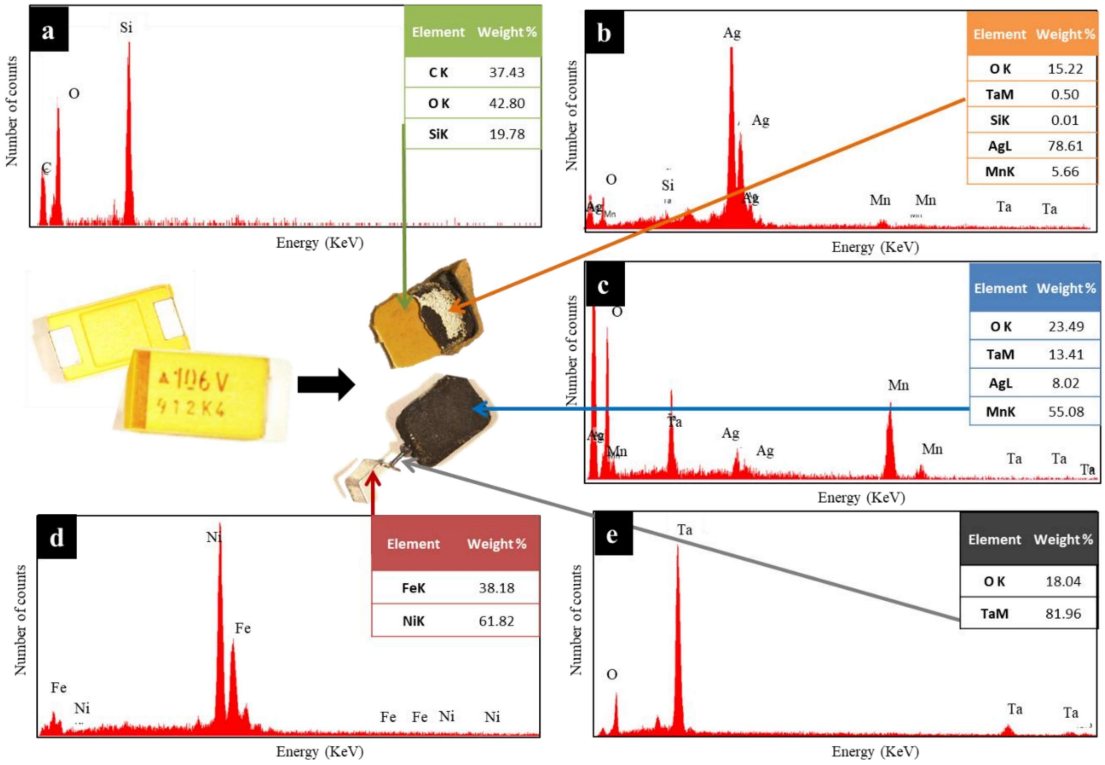

Figure 4.2 Characterization of tantalum capacitor (a) silica-containing mold resin (b) metallic silver, manganese layer (c) Ta anode (d) Ta wire (e) nickel & iron terminal

The images of the capacitor before and after dismantling it and the EDS spectrum collected from different parts are shown in *Figure 4.2*a-e. The EDS from the central part of the capacitor (*Figure 4.2*c) shows that it is made of sintered compact of high-grade tantalum powder (acts as an anode) and tantalum oxide (Ta_2O_5) (dielectric layer). In the middle of this anode, a tantalum wire is inserted (*Figure 4.2*e), which is welded to an iron-nickel alloy terminal (*Figure 4.2*d) at the outer surface. Above this, a layer of MnO_2 is applied, followed by silver and graphite contact as a cathode (*Figure 4.2*b). This entire assembly is encapsulated in epoxy resin embedded with SiO_2 (*Figure 4.2*a) to provide desired mechanical strength to the capacitor. Hammering allows separation of the organic matter from the tantalum-rich product easily.

4.2 Recovery of tantalum from metal-rich concentrate (ERTC)

4.2.1 Alkaline leaching

As a previous researcher reported dissolution of tantalum in basic media falls in the order of Li<Na<K<Rb<Cs (Shikika et al., 2020), we chose the potassium for leaching of tantalum from the capacitor. It is reported that >82% of alkali concentration is required to restrain the formation of insoluble tantalum phase (H. Zhou et al., 2005), which is why we have selected 85% KOH solution to ensure the formation of soluble tantalum compounds. Leaching was carried out for 35 minutes of reaction time, 160°C temperature, 7:1 alkali:ERTC ratio, 500 rpm stirring speed. Percentage leaching of individual metals, calculated from AAS results, reveals that approx.70% of tantalum dissolved into the solution along with iron, silver, and a minute quantity of nickel and manganese as shown in *Figure 4.3*.

The reason for the low recovery of tantalum was expected to be either low reaction time, interference of other impurity elements on the dissolution of tantalum, or formation of some insoluble tantalum complex. The glass vessel used to conduct the experiment began to

dissolve (due to acidic silica) under alkaline leaching conditions, which is why we could not exceed the reaction time beyond 35 minutes.

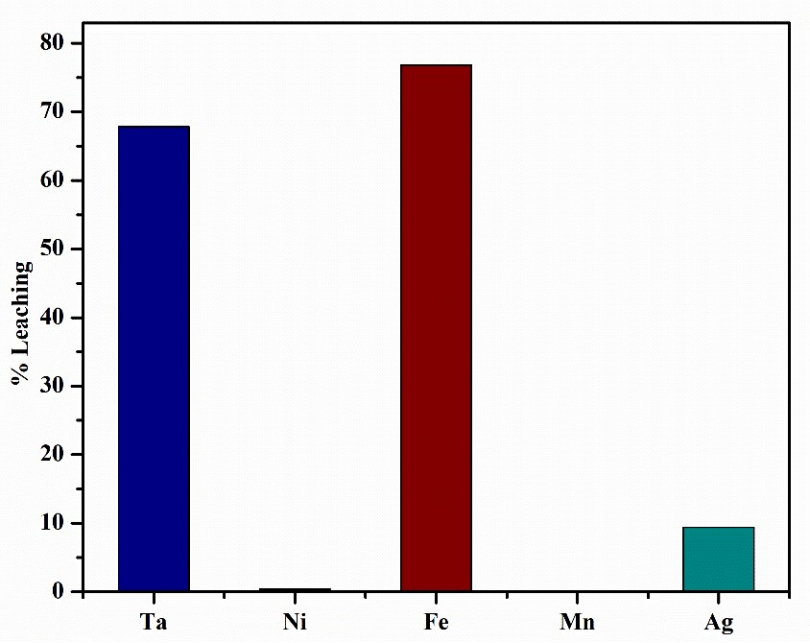

Figure 4.3 Leaching of individual metals in alkaline media (Conditions: 85% KOH, 160°C temperature, 7:1 alkali:ERTC ratio, 35 minutes residence time, 500 rpm agitation speed)

To confirm the reason behind low recovery in leaching, the leached residue was further examined by performing SEM-EDS analysis whose results are illustrated in *Figure 4.4*. The EDS spectrum exhibits a large amount of potassium and tantalum into the residue along with some amount of silica, manganese, and nickel. The presence of such a large amount of potassium into the residue indicated the formation of insoluble tantalum compound during the reaction, as had been reported in previous studies (Wang et al., 2009; H. Zhou et al., 2005; H. M. Zhou et al., 2005). According to the reports, when tantalum is introduced into the aqueous alkaline medium, the decomposition reaction proceeds in two steps. In the first step, tantalum reacts with KOH to form a soluble $K_8Ta_6O_{19}.nH_2O$, and then it transforms to insoluble K_9TaO_3 in the next stage following the reaction shown in *Eq. (4.1) & (4.2),* respectively (H. Zhou et al., 2005; H. M. Zhou et al., 2005). The formation of the

insoluble tantalum phase can be significantly controlled by modifying the operating condition such as the temperature, KOH concentration, solid to liquid ratio etc. as reported in previous literature (Wang et al., 2009; H. Zhou et al., 2005). The content of silica observed in the residue is mainly accounted to the dissolution of glass under such conditions of temperature and basicity.

$$3Ta_2O_5 + 8KOH + (n-4)H_2O = K_8Ta_6O_{19}.nH_2O \quad (4.1)$$

$$K_8Ta_6O_{19}.nH_2O = 6K_9TaO_3 + 2KOH + (n-1)H_2O \quad (4.2)$$

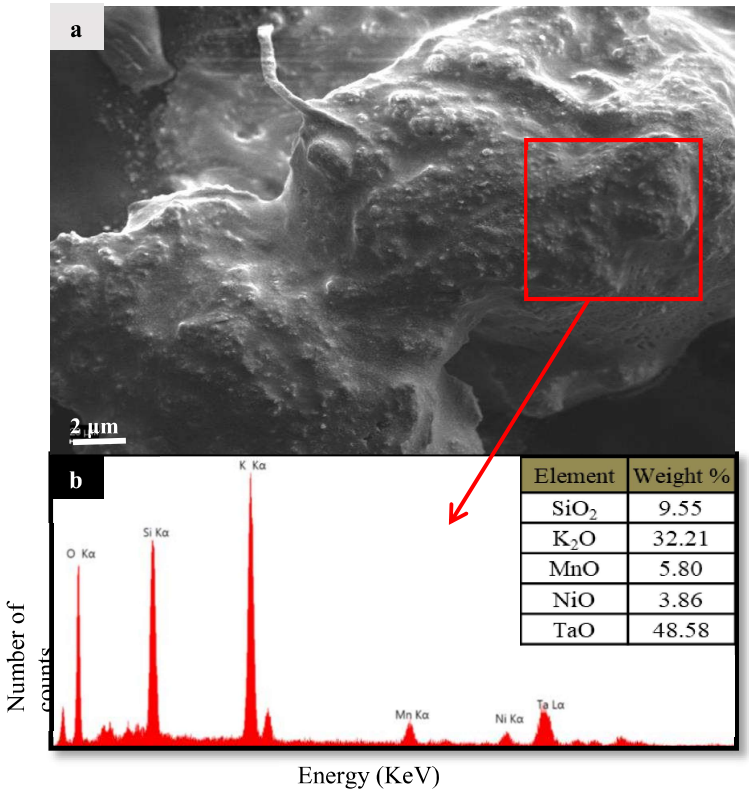

Figure 4.4 (a) SEM morphology and respective (b) EDS spectrum of the obtained residue post alkaline leaching (Conditions: 85% KOH, 160°C temperature, 7:1 alkali:ERTC ratio, 35 minutes residence time, 500 rpm agitation speed)

4.2.1.1 Separaion of tantalum using solvent extraction

After the dissolution of tantalum into the solution, it was further purified by solvent extraction using Aliquat® 336 as a carrier diluted in toluene. To study the effect of pH on

extraction efficiency, different experiments were conducted by varying the pH of the solution from 10-13. Aliquat® 336 exhibit excellent extraction efficiency (>99.5%) in all range of pH. It was found that almost all of the tantalum present in the aqueous phase was extracted at the pH of 11. Extraction of hexatantalate anions using Aliquat® 336 follows an ion-exchange mechanism as reported by Deblonde et al., 2016 (Deblonde et al., 2019; Deblonde et al., 2016). The loaded organic phase was contacted with aqueous HNO_3 for back-extraction of the tantalum. It was found that 4 M nitric acid effectively stripped the tantalum in the solution with >99.99% purity. This purified strip solution can be precipitated and calcined to yield a final Ta_2O_5 product.

4.2.2 Single- stage acidic leaching

In single-stage leaching, silica-free tantalum capacitor was treated using diluted HNO_3 under the following conditions: 3 M HNO_3 as a leaching medium, stirring at 500 rpm, 50°C temperature, pulp density 50 g/l, and for 180 min reaction time. Nickel and iron terminals present in the ERTC could have been separated using magnetic separator before processing the remaining part, but was avoided to minimize the loss of tantalum, as metallic tantalum wire was welded to this terminal. As the reaction proceeds all of the metal start to dissolve except tantalum. After the completion of reaction, the solution was filtered and was analyzed using AAS. Leaching efficiency of all the metals was calculated based on AAS results which are presented in *Figure 4.5*. A large amount of silver (approx. 95%) present in the capacitor dissolved into the leaching reagent along with plenty of nickel (83%) and iron (90.5%) and small amount of manganese (40%). Interestingly a negligible amount of tantalum was dissolved in nitric acid media.

To check the purity of residue obtained after leaching, it was dried in oven overnight, crushed, and then analysed using XRD. Surprisingly, only metallic tantalum peak was detected from the XRD spectrum of the residue (*Figure 4.6*).

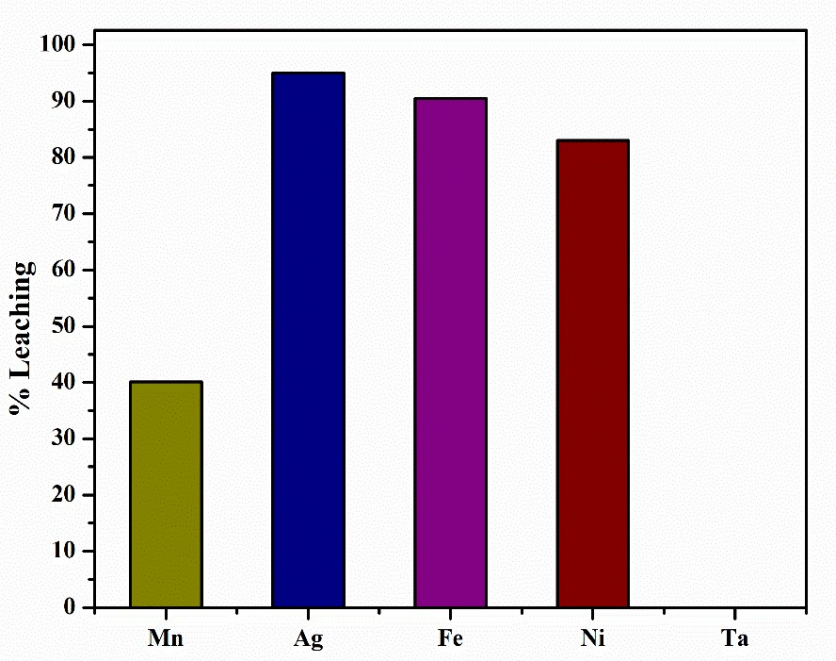

Figure 4.5 Leaching efficiency of different metals in nitric acid leaching (Conditions: 3 M HNO_3, 50°C temperature, 50 g/l pulp density, 3 hour residence time, 500 rpm agitation speed)

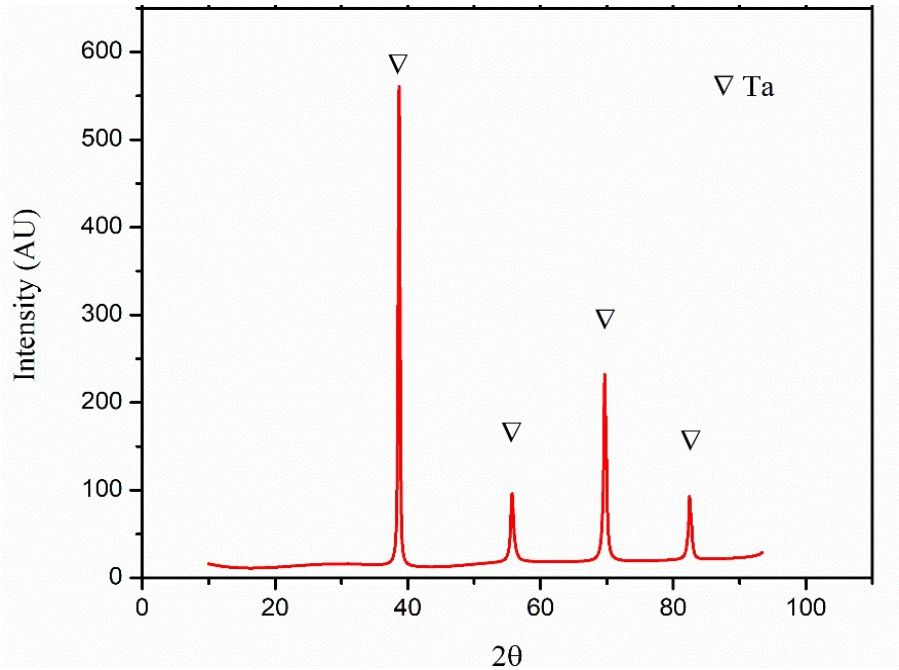

Figure 4.6 XRD pattern of the residue in nitric acid leaching (Leaching conditions: 3 M HNO_3, 50°C temperature, 50 g/l pulp density, 3-hour residence time, 500 rpm agitation speed)

To validate the results obtained in XRD, residue was further characterized with the help of SEM-EDS analysis, whose results are presented in *Figure 4.7*a-b. EDS pattern (*Figure 4.7*b) confirms the presence of metallic tantalum in the residue in an irregular morphology (*Figure 4.7*a). However, along with tantalum large amount of manganese and small amount of iron and nickel were also detected. SEM-EDS analysis reveals that residue contained 27.11% manganese, 0.46% iron, 0.45% nickel, 0.01% silver and rest tantalum.

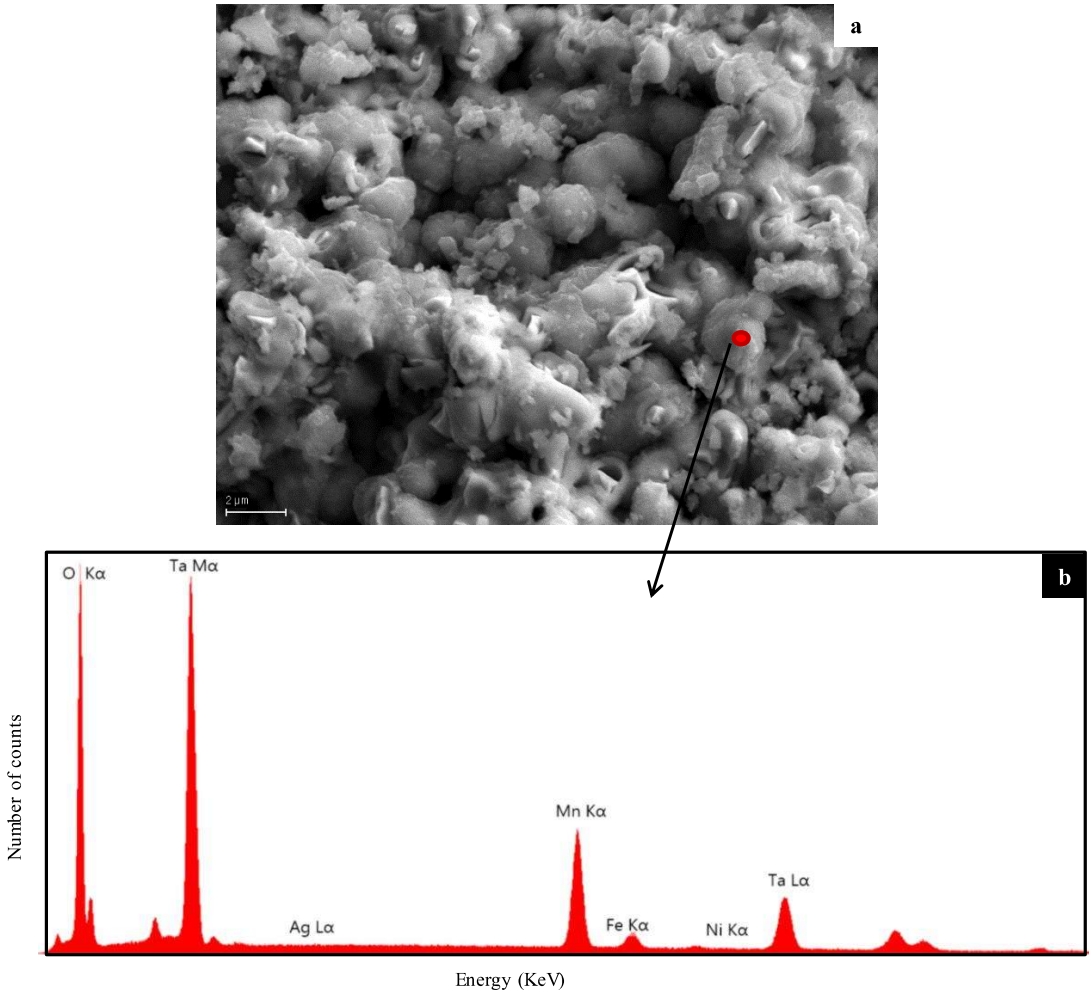

Figure 4.7(a) SEM micrograph and (b) EDS pattern of the residue in nitric acid leaching (Leaching conditions: 3 M HNO_3, 50°C temperature, 50 g/l pulp density, 3-hour residence time, 500 rpm agitation speed)

4.2.2.1 Effect of temperature on manganese leaching efficiency

A considerable amount of manganese was left into the residue compromising the purity of the resultant product. So, the effect of temperature and time was further studied, while keeping the other leaching parameters constant, to arrive at a better condition for dissolution of all the metals excluding tantalum, to get the resultant high purity product. The results are shown in *Figure 4.8*. It can be seen that increasing temperature significantly improved manganese dissolution into the solution with a maximum of 67% at 70°C for 3 h. However, some amount of manganese was always left into the residue, which potentially was due to the passivation of manganese with highly oxidizing nitric acid. As MnO_2 is a stable oxide, a reducing agent was required to dissolve this passivated layer and transform this insoluble Mn(IV) to soluble Mn(II), as had been used in the literature (Lasheen et al., 2009; Sinha and Purcell, 2019). So, it was concluded that nitric acid alone is not sufficient to dissolve all the impurities and get the desired grade tantalum product.

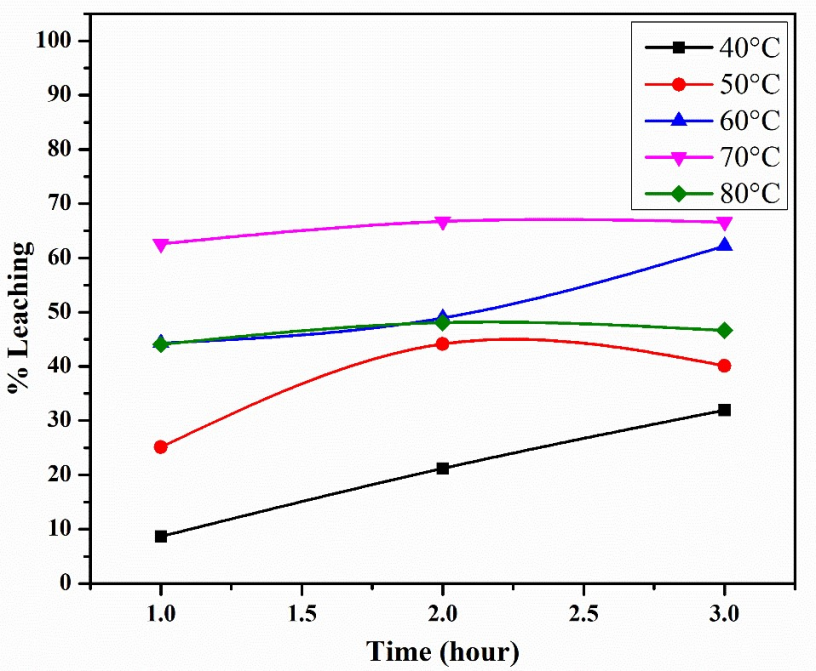

Figure 4.8 Effect of time and temperature on leaching efficiency of manganese in nitric acid leaching (Conditions: 3 M HNO_3, 50 g/l pulp density, 500 rpm agitation speed)

4.2.3 Two- stage leaching

To further improve the purity of final product, a two-stage leaching was developed. In the 1st stage, ERTC was treated with dilute hydrochloric acid (3 M HCl) at 500 rpm stirring speed, 50 g/l pulp density, 50°C temperature, and residence time of 4 h for target removal of manganese and nickel. More than 96% of manganese dissolved in the solution under this condition along with almost complete nickel and large amount of iron. However, silver leaching efficiency was quite low (~27%). Therefore, to dissolve this remaining silver and other minor metals 2nd stage leaching was conducted. For this, the residue obtained was dried in oven overnight and subsequently leached using HNO_3 (3 M HNO_3, 500 rpm, 50°C, pulp density 50 g/l, 3 h). Leaching efficiency of individual metals in both the leaching stage is shown in *Figure 4.9*. Interestingly, in both the leaching stage, dissolution of tantalum into the solution was almost nil. Other metals were dissolved almost completely to yield a final tantalum product with nearly 99.99% purity.

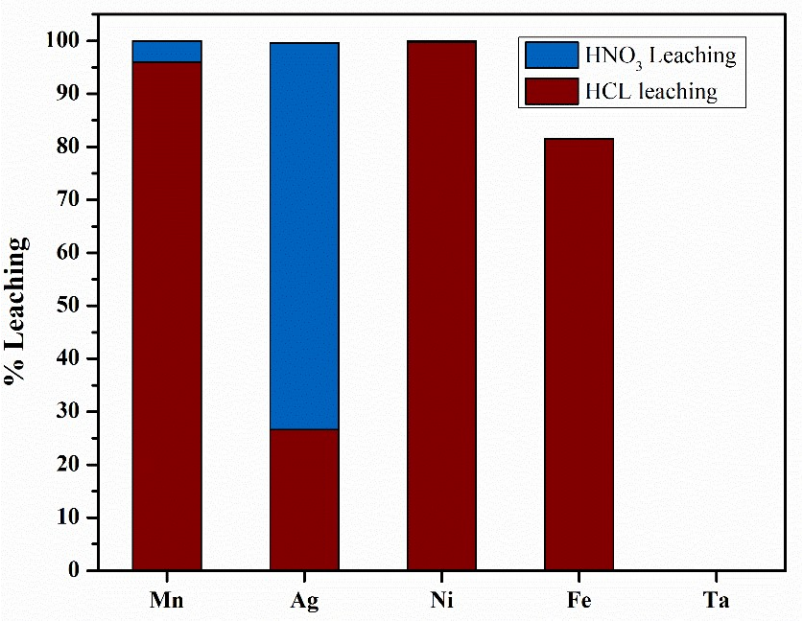

Figure 4.9 leaching efficiency of different metals in stage-1 hydrochloric acid leaching (Conditions: 3 M HCl, 50°C temperature, 50 g/l pulp density, 4 hour residence time, 500 rpm agitation speed)

SEM image and its respective EDS pattern of the obtained residue following this two-stage leaching route are shown in *Figure 4.10*. Only metallic tantalum particles were seen in the residue, corroborating result of AAS, eliminating the further need for any purification step.

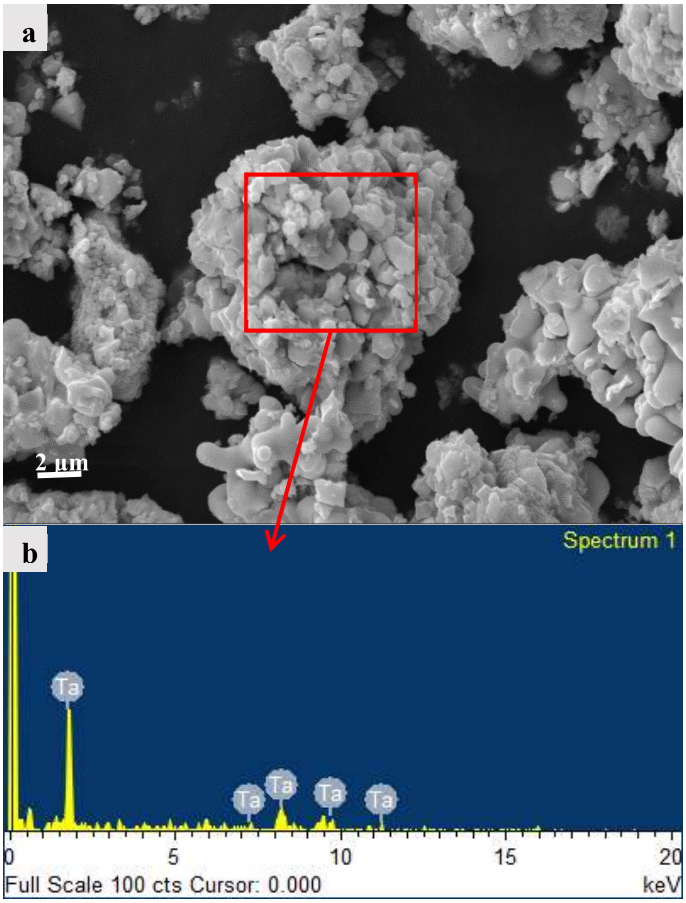

Figure 4.10 (a) SEM morphology and respective (b) EDS spectrum of the obtained residue post double stage leaching (Conditions: stage-1 3 M HCl, 50°C temperature, 50 g/l pulp density, 4 hour residence time, 500 rpm agitation speed; stage-2 3 M HNO_3, 50°C temperature, 50 g/l pulp density, 3 hour residence time, 500 rpm agitation speed)

Weight and composition at various stages of processing the ECTC via the two-stage acidic leaching route has been experimentally determined. On the basis of these results overall flow of material is graphically depicted in *Figure 4.11*. Logit-scale was chosen for the y-axis to better visualize the metals in low concentration. It can be seen that the ECTC is successively enriched at various stages from physically removing the silica resin to

removing metallic impurities in the acidic leaching, to yield a final silica-free tantalum (purity~99.99 wt%).

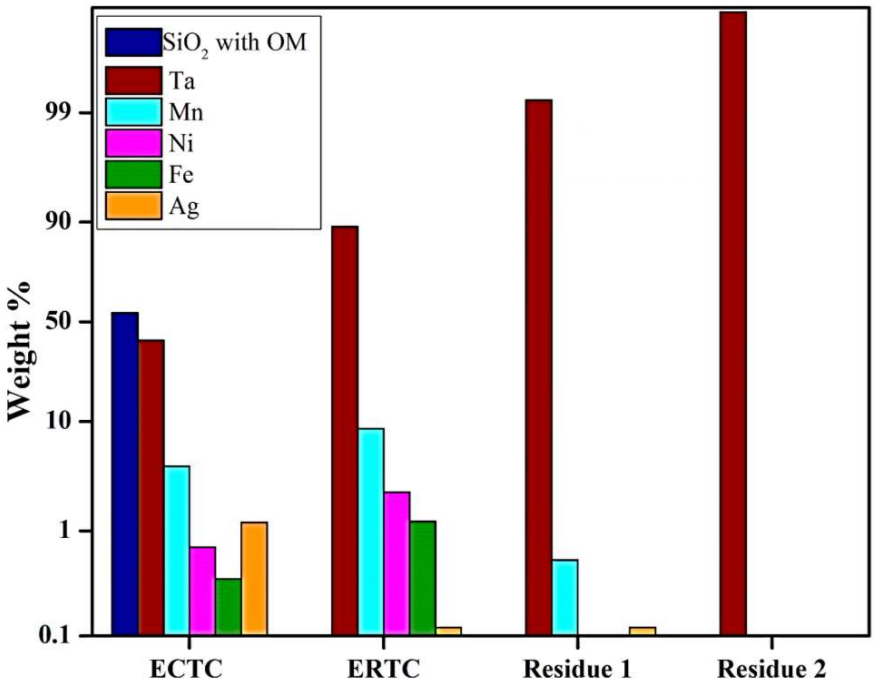

Figure 4.11 Elemental/compound (wt%) at various stages of processing the ECTC via the two-stage acidic leaching route. OM-organic matter, Residue 1- Residue obtained after the first-stage hydrochloric acid leaching, Residue 2- Residue obtained after the second-stage nitric acid leaching

The proposed method is easier and cost-effective than previously established methods (Chen et al., 2019; Niu et al., 2017a). In comparison to expensive and energy-intensive multi-step procedures (Mineta and Okabe, 2005; Niu et al., 2017b; Xia et al., 2021), a considerably simpler pre-treatment step was able to remove 100% of silica. Furthermore, the proposed two-stage acid leaching method produces desired grade tantalum product (purity of 99.99%), obviating the requirement for a purification step and, as a result, lowering additional operational costs. Overall recovery efficiency in the acidic leaching approach was 98%, which was higher than past studies (W.-S. Chen et al., 2022; Mineta and Okabe, 2005; Niu et al., 2017b, 2017d; Xia et al., 2021).

4.2.3.1 Optimization of parameters

To select the most effective condition for leaching of manganese and nickel in 1st stage leaching (HCl leaching) parameters such as temperature, reaction time, pulp density, and concentration of leaching reagent were varied over a range which are described in detail in the following sub-sections.

1) Effect of temperature and reaction time

Figure 4.12 illustrates the time-dependent leaching profile of manganese and nickel at temperatures of 30 °C-70 °C using 3 M HCl, at 50 g/l pulp density, 500 rpm stirring speed, for 240 min. The possible reaction during leaching in given by *Eq. (4.3)* & *(4.4)*. It is evident from the *Figure 4.12* that temperature plays a critical role in the leaching kinetics of both metals, as reported in previous articles too (Muscetta et al., 2021; Rao et al., 2021b). Dissolution of both manganese and nickel increases with the temperature, due to decreased kinetic barrier or increased reaction rate as elevating the temperature elevates the average kinetic energy of the reacting molecules. As a result, a larger fraction of these molecules will possess the required minimum energy for collisions that lead to effective interactions. Reaction rate is maximum at 60 °C, with 99.9%, and 98.9% leaching efficiency for manganese and nickel, respectively. Beyond 60°C, dissolution of both the metals starts to decrease which might be the result of hydrolysis of metal. At a higher temperature, more acid is lost as a result of volatilization. Hence, metal reacts with water and enters into the residue, thus inhibits the further dissolution reaction (Zhang et al., 2016). In addition to that, for a particular temperature (except 30 °C), leaching kinetics was fast over the initial 120 min; thereafter, it slowed down. Therefore, it was inferred that 60 °C temperature and 120 min leaching duration were the optimum conditions to maximize the leaching efficiency.

$$MnO_{2(s)} + 4HCl_{(l)} = MnCl_{2(l)} + 2H_2O_{(l)} + Cl_{2(g)} \uparrow \quad (4.3)$$

$$Ni_{(s)} + 2HCl_{(l)} = NiCl_{2(l)} + H_{2(g)} \uparrow \quad (4.4)$$

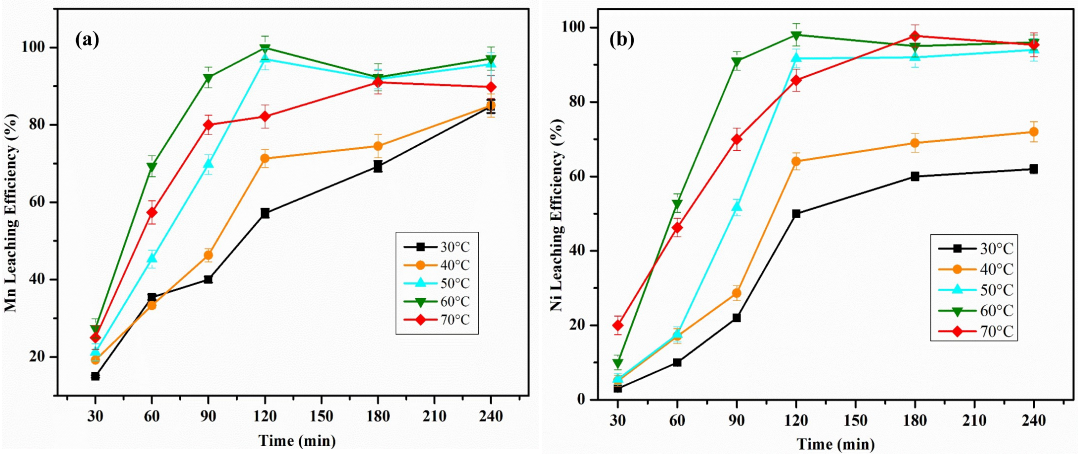

Figure 4.12 Effect of time and temperature on leaching of (a) manganese (b) nickel (Conditions: 3 M HCl, 50 g/l pulp density, 500 rpm agitation speed)

2) Effect of concentration of HCl

Different leaching experiments were carried out to study the effect of chloride concentration (1-3 M HCl) on the dissolution of manganese and nickel under the following conditions: 60 °C temperature, 50 g/l pulp density, and 500 rpm stirring speed for 30-180 min. The measured pH of the prepared solution at each concentration i.e., 1 M, 2 M, and 3 M is 0.23, -0.08, and -0.27, respectively. *Figure 4.13 illustrates* that increasing the molar concentration of the acid led to higher dissolution of manganese and nickel. With 1 M HCl, 85% and 52% of manganese and nickel were dissolved, whereas with 3 M HCl, these metals could be dissolved to 99.9% and 98.9%, respectively. The dissolution of metals could not reach completion at lower HCl concentration even with an extended period of time (180 min). Even though 2 M HCl seemed promising given near complete leaching of manganese, it led to a higher impurity in the resultant tantalum-containing residue due to poorer nickel dissolution (50%). Therefore, a concentration of 3 M HCl was chosen as optimum for the complete dissolution of both the metals.

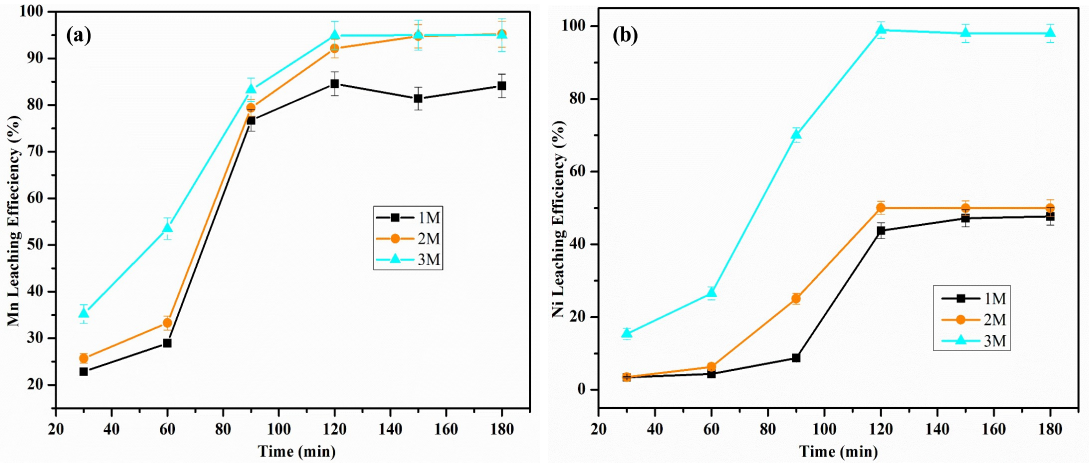

Figure 4.13 Effect of concentration of HCl on leaching of (a) manganese (b) nickel (Conditions: 60 °C temperature, 50 g/l pulp density, 500 rpm agitation speed, 180 min residence time)

3) Effect of pulp density

Finally, the pulp density was varied from 25-100 g/l to evaluate its impact on the leaching efficiency of metals with 3 M HCl, 60 °C temperature, 500 rpm stirring speed, and a leaching duration of 120 min. A gradual increase in manganese dissolution was seen (*Figure 4.14*a) with increasing pulp density. In contrast, nickel dissolution begins to fall at higher pulp density (above 75 g/l) (*Figure 4.14*b) which might be due to ineffective mass transfer and a decrease in residual acid concentration as reported in the previous studies (M. Chen et al., 2015; Rao et al., 2021b). Therefore, for complete dissolution of both the metals, 50 g/l pulp density was considered for subsequent experiments.

The leach liquor produced with these optimized parameters (60 °C, 120 min, 3 M HCl, 500 rpm, and 50 g/l) contained 4300 mg/l manganese, 1485 mg/l nickel, 15.33 mg/l silver, and 7.51 mg/l iron. Quantitative leaching of manganese and nickel were seen along with a large amount of iron, to a lesser extent of silver, and negligible tantalum under these conditions. The residue thus obtained was rich in tantalum (approximately 99% tantalum and 1% impurity elements (manganese, iron, silver, nickel)).

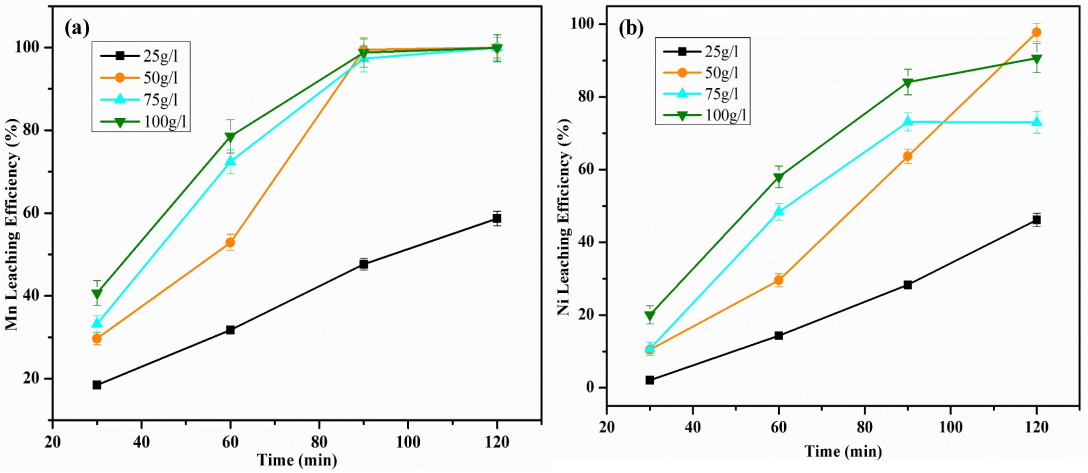

Figure 4.14 Effect of pulp density on leaching of (a) manganese (b) nickel (Conditions: 3 M HCl, 60°C temperature, 500 rpm agitation speed, 120 min residence time)

4.2.3.2 Kinetics of dissolution of manganese and nickel

The study of a kinetic model of leaching allows a much deeper understanding of the mechanism of heterogeneous interaction (liquid leachant and solid feed), which occurs at the solid-liquid interface (Jinyu Wang et al., 2017; Wu et al., 2020). The leaching kinetic for a heterogeneous reaction model can be determined by the popular shrinking core/sphere model or Avrami model (Martínez-Luévanos et al., 2011; Jinyu Wang et al., 2017). In The shrinking core model (*Eq. 4.5*), the diffusion of reacting species through the porous product layer is the rate-limiting step, as against the surface chemical reaction in the shrinking sphere model (*Eq. 4.6*) (Behera and Parhi, 2016). Leaching results shown in *Figure 4.12* were used to examine the validity of the individual models. Here we've applied the shrinking core/sphere model to fit the kinetic data for percentage leaching with temperature and time. The equation used for the diffusion and surface reaction controlled model is given below:

$$1 - \left(\frac{2}{3}\right) x - (1 - x)^{2/3} = k_d . t \qquad (4.5)$$

$$1 - (1 - x)^{1/3} = k_c . t \qquad (4.6)$$

where,

x = fraction of leaching

k_d = kinetic rate constant for the diffusion-controlled reaction

k_c = kinetic rate constant for surface reaction controlled reaction, and

t = reaction time

Data were fitted using both models to determine the kinetic model for the present study and is shown in *Figure 4.15*.

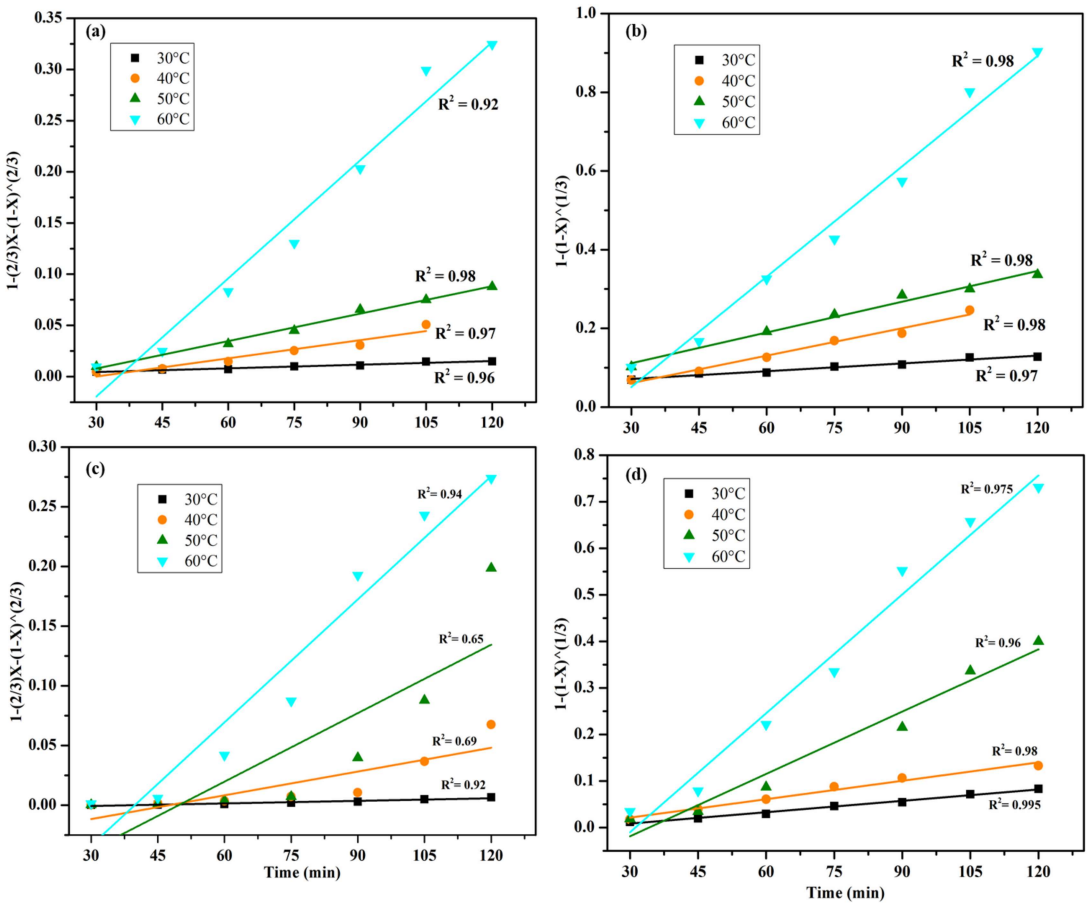

Figure 4.15 Kinetics plots for leaching of manganese for (a) diffusion-controlled model and (b) reaction-controlled model and leaching of nickel for (c) diffusion-controlled model and (d) reaction-controlled model

The kinetic plot illustrated in *Figure 4.15* shows that leaching data for nickel were poorly fitted with diffusion-controlled process model (*Figure 4.15* c) with R^2 value of lower than

0.70 in some cases, whereas for manganese the fitting was marginally better in reaction-controlled process model ($R^2 \geq 0.98$). Kinetic data for nickel were best fitted with reaction-controlled process model with a high correlation coefficient ($R^2 \geq 0.98$) (*Figure 4.15* b & d).

Reaction rate constants kd and kc were then determined from the slope of the linear relationships in *Figure 4.15*. Arrhenius equation (*Eq. 4.7*) was used to establish a relationship between these specific rate constants and temperature, shown in

Figure 4.16, from which the experimental activation energy can be calculated.

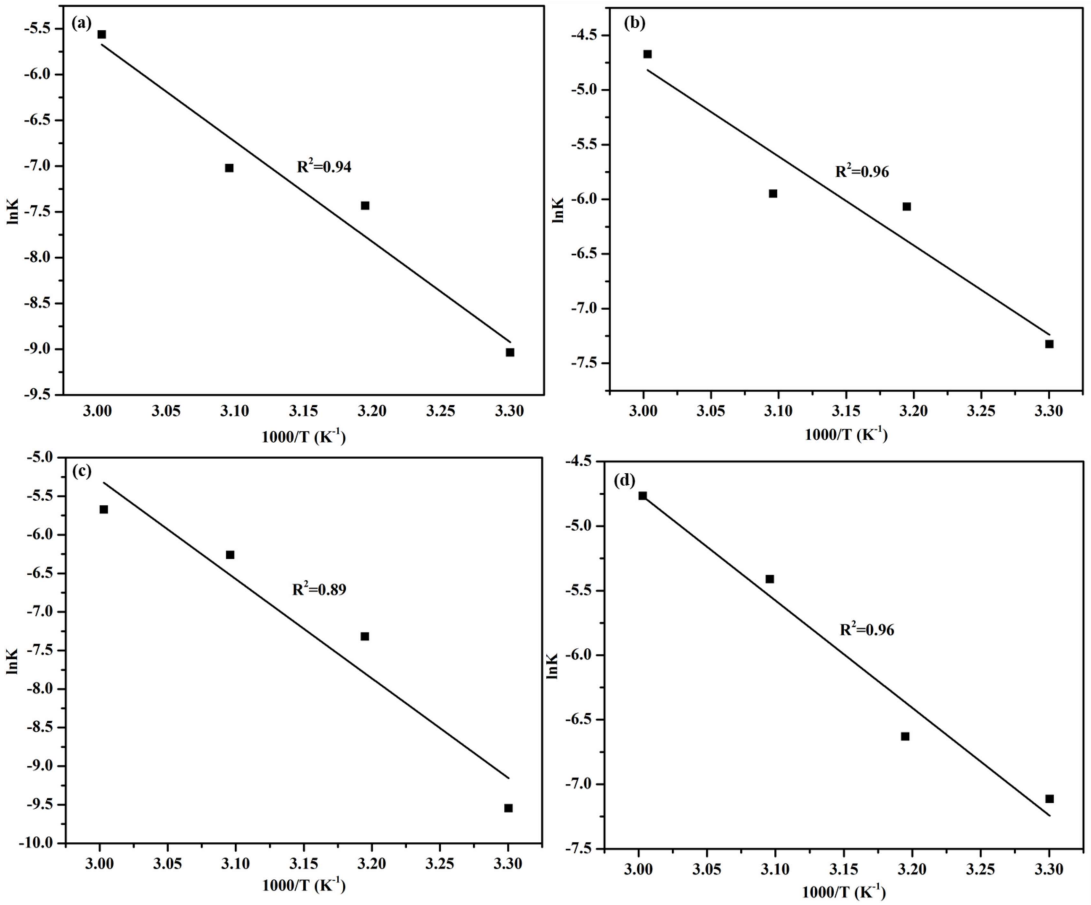

Figure 4.16 Arrhenius plots for leaching of manganese for (a) diffusion-controlled model and (b) reaction-controlled model and leaching of nickel for (c) diffusion-controlled model and (d) reaction-controlled model

$$k = Ae^{(-Ea/RT)} \quad (4.7)$$

where,

k = reaction rate constant

A = pre-exponential factor

E_a = activation energy, and

R = gas constant (8.314 J K^{-1} mol^{-1}).

For a reaction-controlled kinetic model, the activation energy is in the range of 10-20 kcal/mol (41.8-83.7 kJ/mol), while for a diffusion-controlled kinetic model, it is below 10 kcal/mol (Abdel-Aal and Rashad, 2004; Behera and Parhi, 2016). In our case, Ea was calculated to be 67.68 and 69.17 kJ/mol for manganese and nickel, respectively. The obtained activation energy strongly supports that the proposed leaching mechanism is regulated by surface chemical reaction controlled model rather than the diffusion-controlled model.

4.3 Recovery of silver from non-metallic-rich concentrate

4.3.1 Leaching

The solid fraction was leached suing 3 M HNO_3, 50 g/l pulp density, 500 rpm stirring speed, under varying time and temperature. The effect of variation of temperature and time on leaching efficiency of silver is illustrated in *Figure 4.17*. It can be seen that with increase in temperature, the silver leaching efficiency increases. At lower temperature the reaction rate was comparatively slow, and dissolution of silver gradually increases over time from 15-180 min. Whereas, the rate of reaction is very rapid once the temperature was set to 60°C. For just one hour of reaction time, leaching efficiency of silver more than doubled from 42% at 40°C to 97.5% at 60°C. At 60°C, the dissolution rate of silver reaches to the maximum after 90 min reaction time thereafter it remains constant. Therefore, from these experiment 60°C temperature and 90 min of reaction time was taken as optimum for

quantitative dissolution of silver. Along with silver, a large amount of manganese (92%) also entered into the solution and therefore the obtained solution was further subjected to purification to separate the valuable silver.

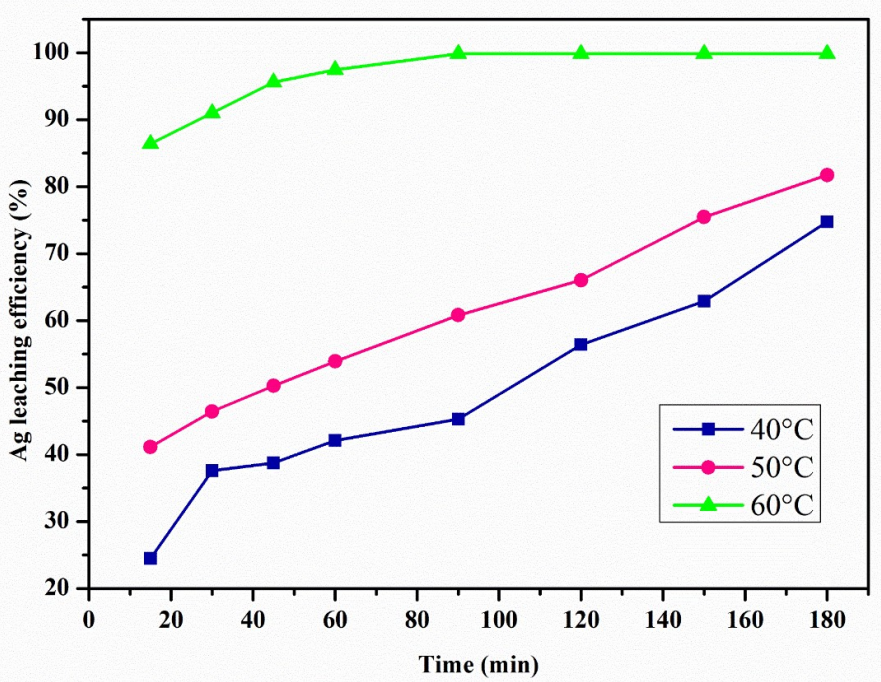

Figure 4.17 Effect of temperature and time on leaching efficiency of silver (Conditions: 3 M HNO_3, 50 g/l pulp density, and 500 rpm agitation speed)

4.3.2 Separation of silver using chemical precipitation

The elemental analysis revealed that, the obtained leach liquor contained 1588 mg/l of silver and 263.8 mg/l of manganese. To concentrate silver from this solution, chemical precipitation method was adopted. Chloride salts were found to be effective for the precipitation of silver from multi-metallic leach liquor (Aktas, 2010; Caldas et al., 2021). Therefore, NaCl powder was used as a precipitating agent to concentrate silver. The amount of NaCl required for complete precipitation of silver was determined from stoichiometric calculation from the given *Eq. (2.4)*.

To ensure quantitative silver precipitation, 100% excess NaCl was used. An immediate reaction was observed with the addition of small amount of NaCl powder and a white

precipitate was settled at the bottom. The addition of powder was continued with constant stirring to avoid any accumulation. After completion of reaction time, the precipitate was filtered and dried for further characterization.

The SEM morphology of the precipitate is shown in *Figure 4.18a*. Through the EDS, the composition of the precipitate was determined which is presented in *Figure 4.18b.* In the EDS spectrum, the presence of Ag and Cl was identified. The presence of Ag and Cl suggests the formation of AgCl in the precipitate. Along with silver and chlorine, only a negligible amount of manganese was detected. No other impurities were detected in the precipitated silver chloride.

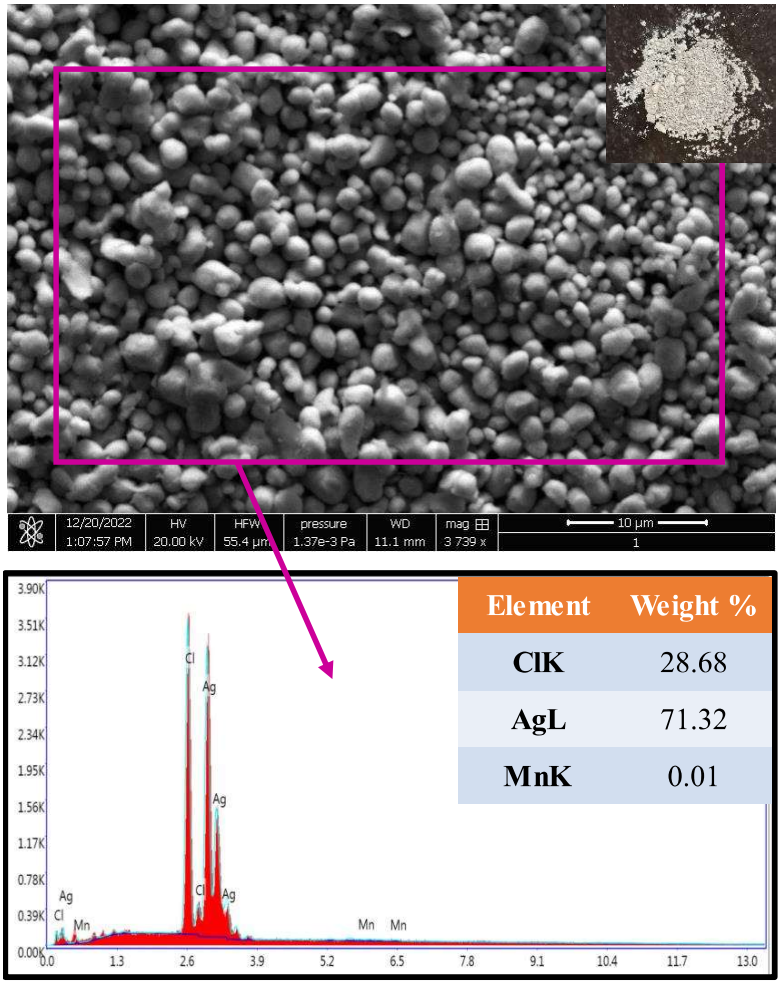

Figure 4.18 SEM-EDS analysis of obtained filtrate after chemical precipitation

To visualize the distribution of elements in the filtrate, elemental mapping analysis was done whose results are illustrated in *Figure 4.19*. It can be seen that, silver and chlorine are widely dispersed throughout the entire region of the precipitate, whereas manganese is sparingly scattered. This distribution confirms the homogeneous composition of the silver throughout the precipitate.

In order to confirm the phases, the precipitate was further characterized by XRD. The peaks were analyzed, which are presented in *Figure 4.20*. The XRD results are in accord with what we found in SEM-EDS analysis. Only silver chloride peaks were identified in the spectrum. Hence this confirms that the precipitate is indeed composed of purified silver chloride.

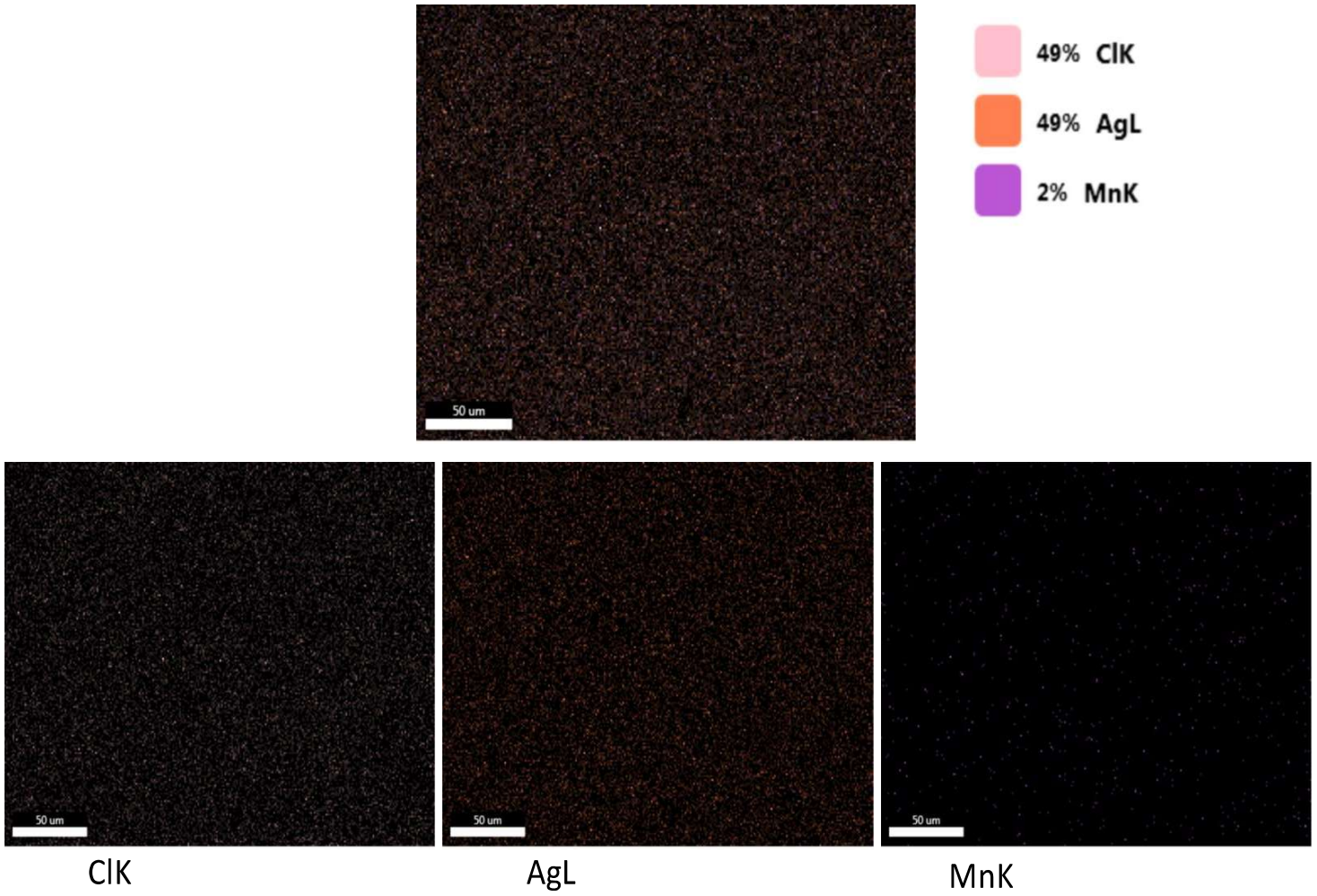

Figure 4.19 Elemental mapping of obtained filtrate after chemical precipitation

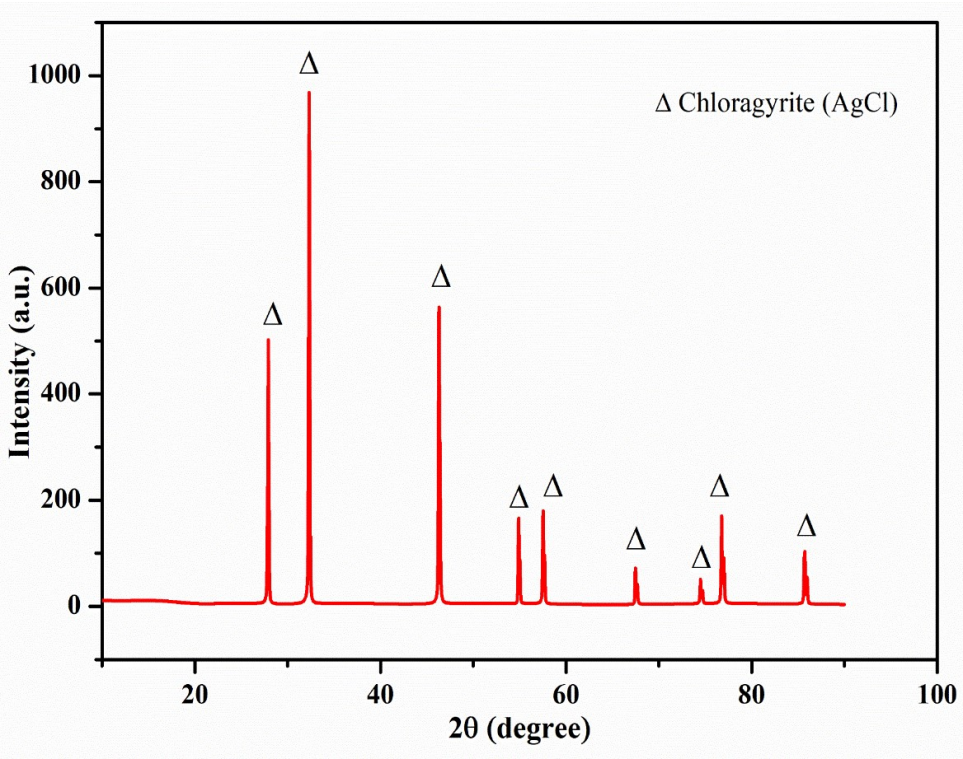

Figure 4.20 XRD pattern of obtained filtrate after chemical precipitation

4.4 Conclusions

In this chapter a hydrometallurgical method was developed for recovery of tantalum and silver from waste tantalum capacitors following different routes. The major outcomes from this chapter is given below:

- A complete silica-free tantalum-rich concentrate is obtained containing ~90% of tantalum along with other metals without need of any energy intensive process.
- Alkaline leaching is a promising method for dissolution of tantalum from waste tantalum capacitors for its subsequent recovery, avoiding the harmful effect of acidic lixiviant.
- Nitric acid alone is not sufficient to recover tantalum by dissolving all other metals into the leaching medium. Large amount of manganese was left into the residue along with tantalum.

- 2-stage leaching is an easier and effective method to dissolve all the metals (except tantalum) into the leachant and concentrating high purity (99.99%) tantalum into the residue.
- 60°C temperature , 120 min reaction time, 3 M HCl concentration, 500 rpm stirring speed, & 50 g/l are the optimized parameters to maximize the recovery of tantalum from metal-rich concentrate.
- Kinetics study shows that leaching of manganese and nickel followed the chemical reaction-controlled model with the activation energy of 67.68 and 69.17 kJ/mol, respectively.
- The benefits of employing acidic media over alkaline ones include greater recovery efficiency, fewer steps, and the absence of an expensive purification step.
- 3 M nitric acid, 60°C temperature, 500 rpm stirring speed, 50 g/l pulp density, and 90 min reaction time are effective for quantitative leaching of silver (99.87%) from non-metallic-rich concentrate. At this condition, majority of manganese (92%) also entered into the solution.
- NaCl is found to be effective reagent for precipitation of silver from leach liquor as silver chloride at room temperature (25°C).
- High purity silver chloride (above 98%) is confirmed in the precipitate from SEM-EDS and XRD results.